Progress In Electromagnetics Research M, Vol. 108, 89–101, 2022

Highly Selective UWB Bandpass Filter with Multi-Notch Characteristics Using Comb Shaped Resonator

Piali Chakraborty[1, *], Partha P. Shome[2], Jyoti R. Panda[1], and Arindam Deb[1]

Abstract—This paper aims to present a highly selective, compact size new ultra-wideband (UWB) bandpass filter with three sharp notches for UWB indoor applications. The fundamental geometry of the filter is based on a modified multi-mode resonator (MMR) structure which comprises an open-ended step impedance resonator (SIR) attached to an interdigitated uniform impedance resonator (UIR). Realizing a Comb-shaped resonator structure below the UIR and symmetrically extending the lower arm edge of the interdigital coupled lines, three notches are generated at 6 GHz, 6.53 GHz, and 8.35 GHz. These notches have improved the UWB bandpass filter responses by suppressing the existing interferences in the UWB passband created by Wi-Fi 6E (6 GHz), super-extended C band (6.425 GHz $\sim$ 6.725 GHz), X band satellite communications for satellite TV networks or raw satellite feeds (7.25 GHz $\sim$ 8.395 GHz). Concurrently the notched band filter has achieved superiority in other salient features concerning passband and stopband of the filter such as a high passband fractional bandwidth (115.76%), low return loss (-13.27 dB), low insertion loss (0.44 dB $\sim$ 0.97 dB), wide upper stopband (5.37 GHz), nearly flat group delay (0.28 ns $\sim$ 0.45 ns), etc. The ultimate design of the UWB bandpass filter is fabricated and verified by comparing the simulated filter responses with the measured results indicating a good agreement.

1. INTRODUCTION

Introducing a vast frequency band of 3.1 GHz to 10.6 GHz for unlicensed commercial use benefiting public safety, consumers, businesses Federal communication commission (FCC) in 2002 has unrolled a tremendous opportunity for researchers of ultra-wideband (UWB) technology [1]. UWB devices are applicable in different imaging systems (wall, through wall, medical), different radar systems (ground penetrating, surveillance, vehicular), and in communication and measurement systems that include handheld devices like laptop, personal digital assistant (PDA), etc. and devices for high-speed indoor networking applications. Since the beginning, substantial research works have been proceeding to construct the microwave circuits associated with UWB devices, especially ultra-wideband bandpass filter which is an essential unit of the UWB communication systems. Achieving good bandpass filter responses satisfying FCC specified standard, while operating at the center frequency (6.85 GHz) and prevailing a fractional bandwidth (FBW) of 110%, was a huge challenge in earlier days. However, the continuous attention of researchers in this field, whether in the establishment of novel methods or modification of existing techniques, made it possible to enhance the FBW from 40%–70% to greater than 110% in recent days [2]. Researchers have been establishing different methods to design UWB bandpass filters not only for satisfying the filter frequency band and emitted power level restriction but to improve filter fractional bandwidth, insertion loss, return loss parameters, and group delay simultaneously, for instance, application of coupled meandered line [3], generating unit

Received 26 November 2021, Accepted 28 January 2022, Scheduled 16 February 2022

* Corresponding author: Piali Chakraborty (chakraborty.piali1987@gmail.com).

[1] School of Electronics Engineering, Kalinga Institute of Industrial Technology, Bhubaneswar 751024, India. [2] Department of ECE, Dr. B R Ambedkar National Institute of Technology, Jalandhar 144011, India.

cell from composite right-/left-handed transmission line [4], hybrid structure combining microstrip and coplanar waveguide [5], asymmetric parallel-coupled line [6], multimode resonators (MMR) [7–10], composite highpass/lowpass filter topology [11], defected ground technology [12], complementary split-ring resonator (CSRR) [13], multilayer aperture coupled patches [14], etc. Employing very short duration (0.1–2 ns) pulses for transmitting information allows UWB filter a large emission bandwidth which in turn guards UWB signal against the interference generated by other licensed pre-existed radio services like WLAN (5.8 GHz), WiMAX (3.5 GHz), and satellite communication (8 GHz). But day by day increasing spectrum demand, huge traffic issues further bring the researchers to take extra precaution against spurious signals by introducing a notched band centering other radio operational frequencies. Many research works have been conducted to design single or multiple notch band UWB bandpass filters. Notches are generated mostly by loading horizontal or vertical free stubs or stepped impedance resonators or other resonators at a proper position in the original structure. For example, the coupling of SIR to the distributed highpass filter cascaded with an elliptical lowpass filter brings a notch at 5.22 GHz [15]. A composite right/left-handed transmission line UWB filter achieved double notch bands at 4 GHz and 7 GHz by adding L-shaped strip lines on either side of the filter [16]. Some designs have investigated a tri-layer technology to obtain the notch at the desired frequency. In [17], the addition of a U-shaped resonator in the middle layer accompanied by the top layer and bottom layer served the purpose. The filter in [18] achieved a transmission zero at 5 GHz by an open and short-circuited parallel-coupled line structure. Despite circuit complexity, the microstrip to coplanar waveguide transition method is also explored for notch creation namely by loading folded split ring resonators near feed lines also by using spiral resonators and FSSR on the sectoral defected ground structure [19, 20]. Another well-implemented structure is an MMR-based structure which is popular for its design simplicity. Employing a stub-loaded microstrip resonator with exponentially tapered impedance line (ETILSLMR) in MMR-based UWB filter can introduce a notch at 5.5 GHz [21]. In [22], an MMR structure is loaded with an external microstrip triangular loop resonator for notch generation. From the above literature study, it can be noticed that all methods have some limitations in performance in terms of circuit size, complexity, loss characteristics, group delay, etc. So, this paper intends to develop an MMR-based UWB bandpass filter that can facilitate notch functionality centered at Wi-Fi, C band, and X band operating frequency ensuring sharp removal of the interference signal.

This paper introduces 1) a new comb-shaped resonator structure embedded in a basic MMR-based UWB filter to incorporate RF band suppression capability by producing notches at relevant frequencies, 2) analysis of the comb resonator by equivalent circuit model along with corresponding graphical corroboration to explain the notch generation mechanism transparently, 3) and an additional method that is employed in the basic structure to usher notches to the design that is the downward extension of the lower arm edges of the interdigital coupled lines. Hence, a compact triple notched band UWB bandpass filter is put forward without any design complexity. Here Section 2 covers the design structure and simulation results of the plain UWB bandpass filter. Section 3 shows the modified design framework of the UWB bandpass filter by generating notches along with the obtained simulation results, and Section 4 deduces the conclusion.

2. BASIC MMR-BASED UWB BANDPASS FILTER

2.1. Basic Principle of the Microstrip Resonators Required to Design the Proposed UWB Bandpass Filter

The basic UWB filter presented in the paper is based on a multimode resonator structure which comprises a uniform impedance resonator (UIR) and a stepped impedance resonator (SIR). In the context of the proposed filter design, basic structure of half-wavelength UIR and $\lambda_g/4$ type of SIR are discussed here. The stripline conductor, UIR, possesses uniform width through the overall length which is half-wavelength of the dielectric substrate material. Resonances of UIR occur periodically at the frequencies which are integer multiple of the fundamental resonant frequency. On the other hand, the SIR structure comprises a transmission line having open-ended and short-ended line sections with a step junction joining them. The circuit has input impedance Z_i and input admittance $Y_i(= 1/Z_i)$. Fig. 1 depicts different parameters of UIR and SIR structures where Z_1 and Z_2 indicate two transmission line

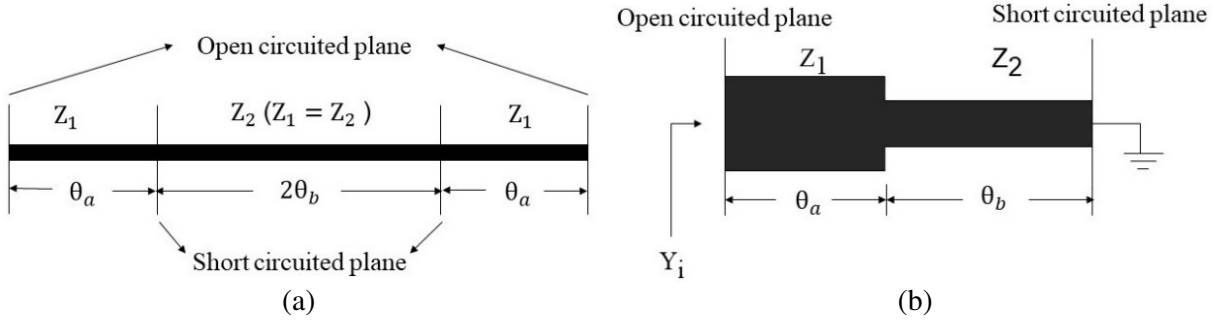

Figure 1. Variation in configuration of various resonators used in the basic UWB filter design: (a) half-wavelength uniform impedance resonator (UIR), (b) quarter wavelength stepped impedance resonator (SIR).

impedances with electrical lengths θ_a and θ_b, respectively. So, Z_i can be determined as:

$$Z_i = jZ_2 \frac{Z_1 \tan\theta_b + Z_2 \tan\theta_a}{Z_2 - Z_1 \tan\theta_a \tan\theta_b}. \tag{1}$$

For parallel resonance condition $Y_i = 0$, Equation (1) can be expressed as:

$$Z_2 - Z_1 \tan\theta_a \tan\theta_b = 0. \tag{2}$$

Thus,

$$\tan\theta_a \tan\theta_b = Z_2/Z_1. \tag{3}$$

Equation (3) defines a critical parameter, impedance ratio which performs a significant role in controlling the resonance of the structure. The impedance ratio of UIR is unity as characteristics impedances of the line sections are equal [23].

2.2. Design of UWB Bandpass Filter

The structural layout of the UWB bandpass filter containing both top view and bottom view in a single composition is portrayed in Fig. 2. A multimode resonator (MMR) excited through interdigital coupled lines is the fundamental element that forms the top layer. On the other hand, the bottom layer is furnished with two rectangular-shaped apertures, etched underneath the interdigital coupled

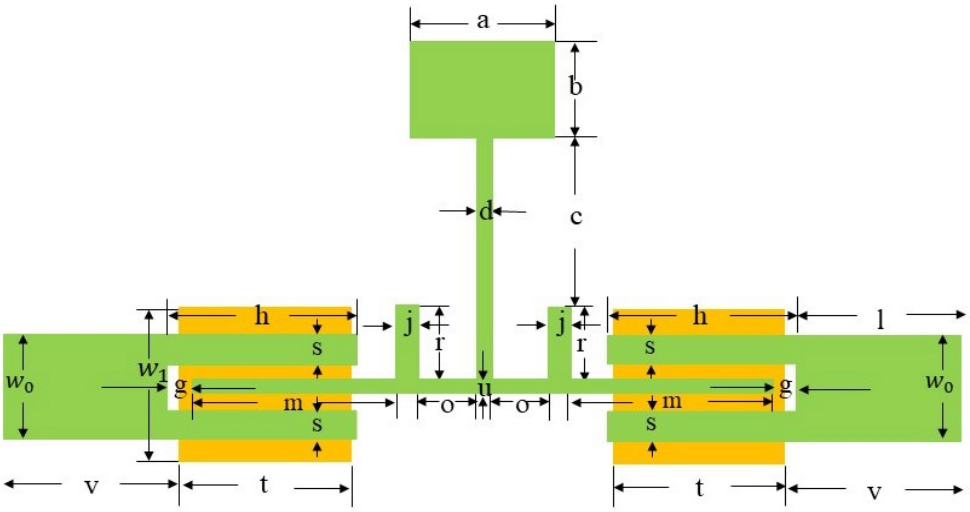

Figure 2. Structural view of the proposed basic UWB bandpass filter.

line arms enhancing the coupling between input/output port and the MMR structure by degrees. The configuration of MMR for the proposed design is accomplished by loading a stepped impedance resonator (SIR) at the center position of a uniform impedance resonator (UIR) along with two vertical open-ended stubs, which are equidistant from the SIR on both sides. The ultimate broad passband of this filter is molded from the first four resonance peaks, which occurred due to this structure. The proposed MMR layout facilitates a good impedance matching within the passband as well as suppression of spurious resonance outside the passband. Dimensions of all optimized filter elements measured in mm are mentioned below:

$a = 4.66$, $b = 3.86$, $c = 5.75$, $d = 0.8$, $g = 0.21$, $h = 7.71$, $j = 0.9$, $l = 3$, $m = 8.52$, $o = 1.28$, $r = 3.38$, $s = 0.64$, $t = 6.4$, $u = 0.5$, $v = 3.61$, $w_0 = 2.2$, $w_1 = 3.3$.

2.3. Analysis of Multimode Resonator

Due to the symmetrical structure, the MMR of proposed design can be analyzed by separating the MMR structure in even and odd modes. Fig. 3(b) and Fig. 3(c) respectively display the equivalent circuits of even mode and odd mode excitation, characterized by the electrical lengths and characteristic admittance of the transmission line segments. The physical length and width of the transmission line sections contribute to calculating the electrical lengths and characteristic admittances. There are three segments in odd mode with electrical lengths θ_1, θ_2, θ_3, and characteristic admittances Y_1, Y_2, Y_3 [24]. The input admittance represented by $Y_{in,\,odd}$ can be expressed as:

$$Y_{in,\,odd} = Y_1 \left(Y_{in2} + jY_1 \tan\theta_1\right) / \left(Y_1 + jY_{in2} \tan\theta_1\right) \tag{4}$$

where $Y_{in3} = -jY_3 \cot\theta_3$ and $Y_{in2} = Y_2(Y_{in3} + jY_2 \tan\theta_2)/(Y_2 + jY_{in3} \tan\theta_2)$.

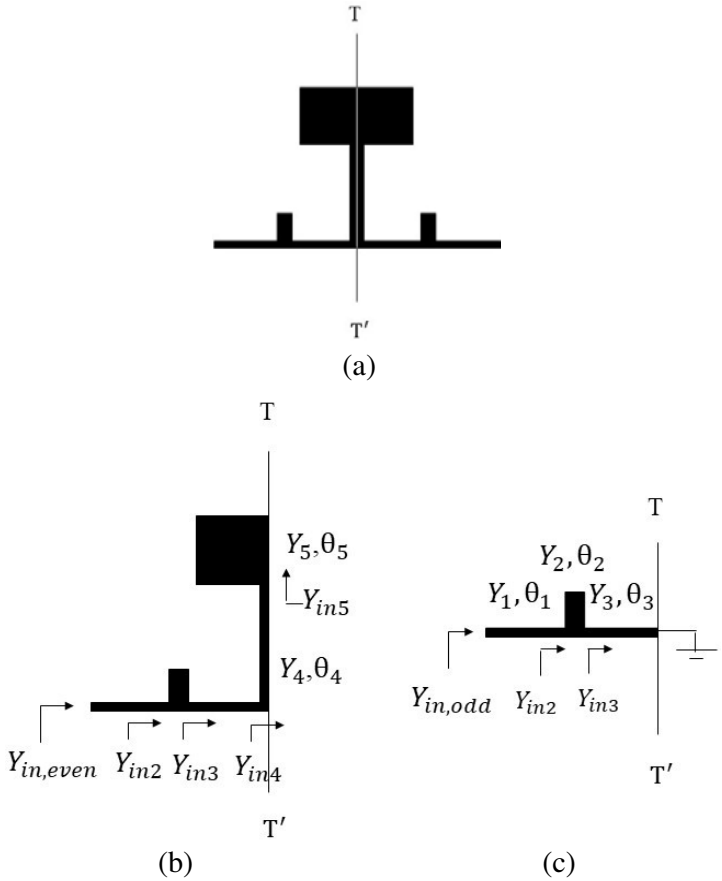

Figure 3. (a) Multimode resonator configuration (MMR) of proposed design, (b) even mode, (c) odd mode.

Considering the operating frequency range from 1 GHz to 20 GHz, Equation (4) determines the input admittance which brings two resonant frequencies f_1 and f_3 for odd mode. Similarly, for even mode analysis, the structure is divided into five different segments having characteristics admittances from Y_1 to Y_5 and electrical lengths from θ_1 to θ_5. Input admittance for even mode can be calculated from Equation (5).

$$Y_{in,even} = Y_1 \left(Y_{in2} + jY_1 \tan\theta_1\right) / \left(Y_1 + jY_{in2} \tan\theta_1\right) \tag{5}$$

where $Y_{in2} = Y_2(Y_{in3} + jY_2 \tan\theta_2)/(Y_2 + jY_{in3} \tan\theta_2)$, $Y_{in3} = Y_3(Y_{in4} + jY_3 \tan\theta_3)/(Y_3 + jY_{in4} \tan\theta_3)$, $Y_{in4} = Y_4(Y_{in5} + jY_4 \tan\theta_4)/(Y_4 + jY_{in5} \tan\theta_4)$, and $Y_{in5} = jY_5 \tan\theta_5$.

From the calculation of even mode input admittances, at operating frequency range, 1 GHz–20 GHz, two even mode resonant frequencies such as f_2 and f_4 are achieved for each resonator length variation. Resonator characteristics of the design are explained in Fig. 4 where Fig. 4(a) shows the changes in odd mode resonant frequencies with respect to the changes in vertical stub length 'r' along with its distance 'o' from the central stub of SIR. Here 'r' is varied from 0 mm to 4 mm for three cases of stub location such as 'o' = 0.88 mm, 'o' = 1.28 mm, and 'o' = 1.68 mm. As a result of these variations first odd mode resonant frequency f_1 shifts slightly upward, but the second odd mode resonant frequency f_3 changes prominently over the stub length which means that f_3 is shifted from higher frequency to lower frequency following the increment in stub length 'r'. Thus, this stub exploits the first and third resonant modes of MMR in creating a wide passband. Fig. 4(b) shows the nature of even mode resonant frequencies based on the open-ended stub of the stepped impedance resonator. An increment in stub width 'b' in accordance with the length 'a' transfers the higher order resonant peaks to a comparatively lower frequency within the UWB passband. As the bandwidth is dependent on the separation between the resonant frequencies, with the manual optimization of stub width by increasing the value of 'b' from 0.6 mm to 3.38 mm, the maximum achievable bandwidth is obtained.

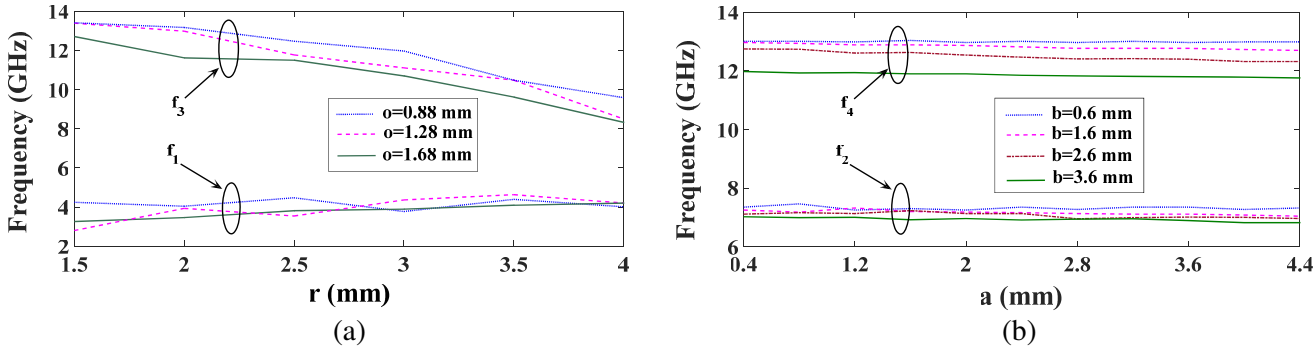

Figure 4. Response of resonance frequencies according to variation in resonator length, (a) response of odd mode resonant frequencies, (b) response of even mode resonant frequencies.

2.4. Simulation Results

The bandpass filter of this paper is constructed, simulated, and analyzed by HFSS V13 software [25]. The substrate Arlon of relative dielectric constant 2.5 along with thickness 0.8 mm is chosen for this purpose. The standard transmission characteristics of a bandpass filter equally depend on the element selection together with a strong coupling establishment between them. The effect of the coupling between input/output ports and the MMR structure is demonstrated in Fig. 5 and Fig. 6. Progressive response of the insertion loss characteristics curve ($|S_{21}|$) of UWB bandpass filter is illustrated in Fig. 5 where the insertion loss is observed to get lower simultaneously with increment in the degree of coupling. Coupling capacity can be enhanced by varying the interdigital coupled line length 'h'. Optimizing 'h' from 0.2 mm to 7.71 mm can remove a 49.62 dB insertion loss by allowing the filter to be operated under a transition from minimum coupling to strong coupling. Five resonance frequencies are obtained by this design to form a wide passband that can be noticed under minimum coupling conditions with the value of 'h' being 0.2 mm. Resonance frequencies are noted as f_i = 3.38 GHz, f_1 = 4.91 GHz, f_2 = 7.3 GHz, f_3 = 9.21 GHz, f_4 = 10.6 GHz. Among five resonances the initial resonance f_i, which

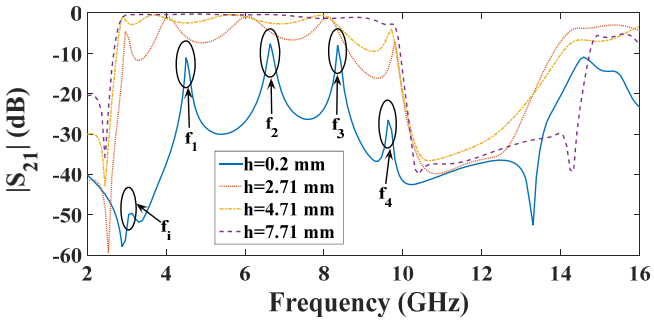

Figure 5. Magnitude of $|S_{21}|$ for weak coupling conditions.

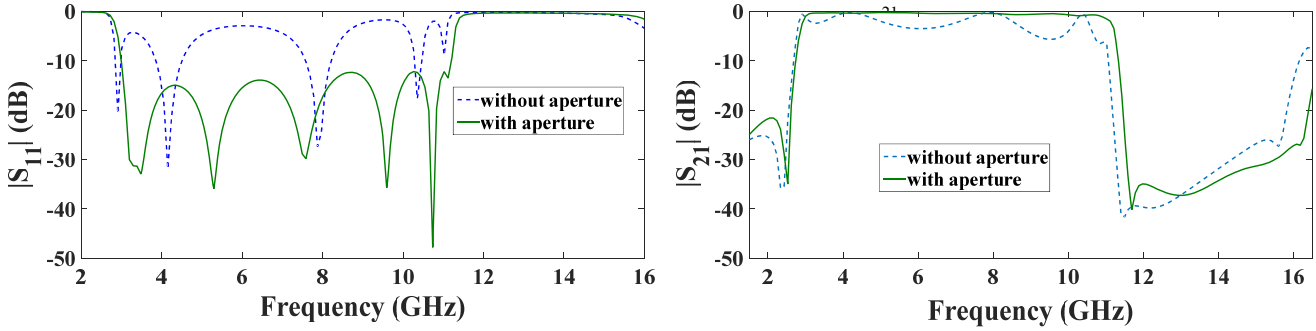

Figure 6. Response of S parameters with and without using apertures, (a) variation in magnitude of $|S_{11}|$, (b) variation in magnitude of $|S_{21}|$.

occurs at 3.38 GHz, is contributed by the perfect coupling between the interdigital couple lines and the MMR structure while the remaining four successive resonances such as f_1, f_2, f_3, f_4 are fetched solely by the optimized MMR configuration presented in Fig. 2. These four resonant frequencies, obtained from the simulation process in HFSS software, have exhibited a good similarity with the resonances deduced from the equivalent circuit model analysis of MMR composition performed in MATLAB software as illustrated in Subsection 2.3. The necessity of aperture arrangement for good filter performances in terms of establishing a good impedance matching between two ports is shown in Fig. 6. The influence of the presence of two properly shaped aperture in the ground plane beneath the interdigital line is observed in reduced loss levels of $|S_{21}|$ and $|S_{11}|$ curves. The return loss referred to in Fig. 6(a) is noticed to be reduced from -3.07 dB to -12 dB, and the insertion loss is reduced to a maximum level of 6.13 dB as shown in Fig. 6(b).

Finally, overall, in-band and out of band filter performances are inspected in Fig. 7(a). The passband created by the proposed bandpass filter is stretched from 2.86 GHz to 11.2 GHz that is a broad passband of 8.34 GHz. A low return loss of -12.22 dB is noticed from the magnitude variation of the $|S_{11}|$ curve. Similarly, a small insertion loss (0.25–0.6 dB) is calculated from the magnitude variation in the $|S_{21}|$ curve. The appearance of transmission zeros at the lower passband edge that is at 2.52 GHz with attenuation -34.96 dB and at the upper passband edge that is at 11.69 GHz with attenuation -40.17 dB facilitates the filter to exhibit a keen changeover both from stopband to passband and from passband to stopband. Thus, high frequency selectivity should be an essential characteristic of a bandpass filter to be able to reject the spurious signal outside the passband sharply. Apart from the passband attributes, a standard stopband property is also displayed by the filter such as a lower stopband extending from 0 to 2.61 GHz and a 4.94 GHz wide upper stopband extending from 11.47 GHz to 16.41 GHz with rejection level -20 dB. The effective consumed area by this filter is limited to $0.81\lambda_g \times 0.51\lambda_g$. The group delay plot is nearly flat all over the passband as indicated in Fig. 7(b), and it differs between 0.23 ns and 0.32 ns.

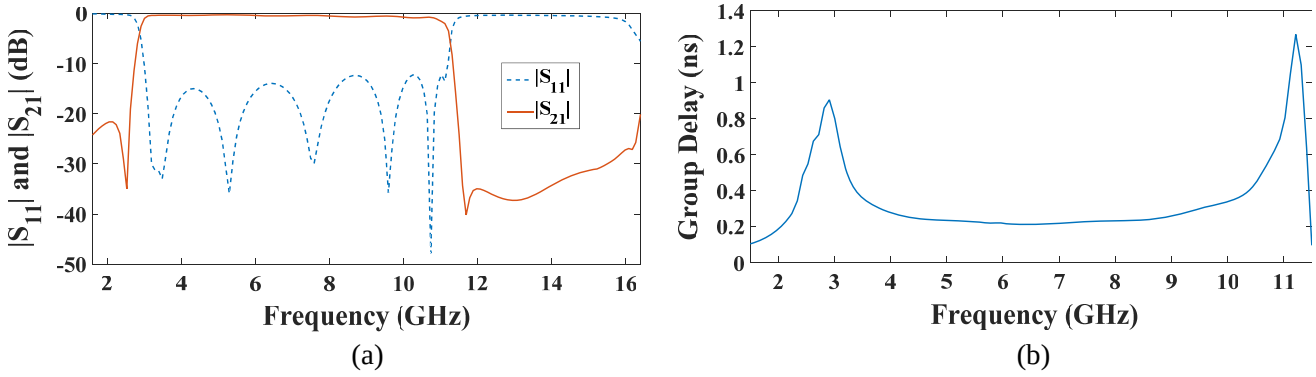

Figure 7. Simulated output of the proposed basic UWB bandpass filter, (a) magnitude of $|S_{11}|$ and $|S_{21}|$, (b) group delay.

3. UWB FILTER RESPONSE IMPROVEMENT BY NOTCH GENERATION

3.1. Design of Proposed Notched Band UWB Bandpass Filter

The modification and up gradation in the structural layout of the proposed UWB bandpass filter introduced in Fig. 2 enable the filter to generate three notches for suppressing the Wi-Fi, C band, and X band spurious radio signals present in the passband. The substrate top view and bottom view of ground plane are combined in Fig. 8. Two methods are realized to generate the notches namely the loading of a comb-shaped resonator below the uniform impedance resonator and the downward one arm extension of the interdigital coupled lines connected to both input and output ports. All the optimized dimensions of the filter elements measured in mm are noted below:

$d = 0.8$, $e = 4.4$, $f = 3.68$, $g = 0.21$, $h = 7.71$, $i = 0.3$, $j = 0.9$, $k = 6.2$, $l = 3$, $m = 8.52$, $n = 0.2$, $o = 1.28$, $q = 1$, $r_1 = 5.55$, $r_2 = 3.9$, $r_3 = 1.4$, $r_4 = 5.8$, $s = 0.64$, $t = 6.4$, $u = 0.5$, $v = 3.61$, $w_0 = 2.2$, $w_1 = 3.3$, $x = 0.2$, $y = 0.4$, $z = 0.5$.

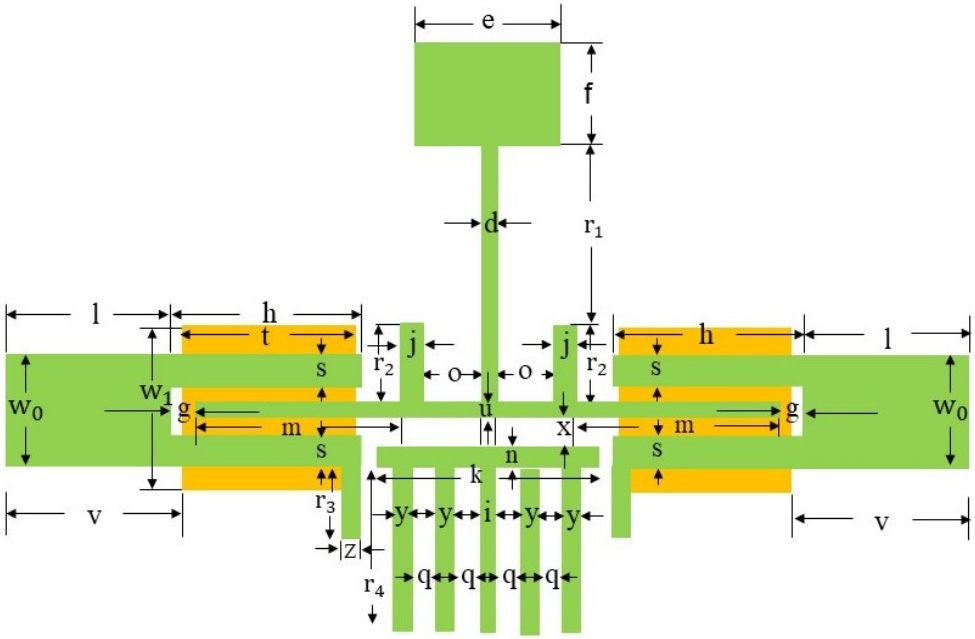

Figure 8. Structural view of the proposed notched band UWB bandpass filter.

3.2. Equivalent Circuit of Comb Resonator and Proposed Filter Structure Incorporating Notch Generating Tools

The comb-shaped resonator embedded in the plain UWB bandpass filter layout has enriched the filter performance by contributing two notches to the output characteristics. One notch is obtained at 6.53 GHz and the other at 8.35 GHz. But the rejection level of the X band suppressing notch acquired by this method was not satisfactory, so another notch generating method is introduced simultaneously that is a downward extension of the lower arm edge of interdigital couple line both on the input and output sides. This measure not only improves the attenuation level of the aforementioned notch also leads to a notch at 6 GHz with a dip in attenuation. In addition to establishing the functional potency of the comb resonator by simulation process, an equivalent circuit model analysis of the resonator is also presented to explain the notch generation mechanism vividly. Though the resonator geometry can be analyzed for both the cases of even mode and odd mode excitation, it is noticed that the obtained resonance (18 GHz) from the even mode analysis is well exterior from the passband span. Hence, only the odd mode analysis is provided in detail. From the odd mode equivalent circuit of the comb resonator, as delineated in Fig. 9(a), resonance for the notch is obtained within the UWB passband. Here the equivalent circuit analysis process is the same as that adopted in Subsection 2.3. Comb resonator circuit

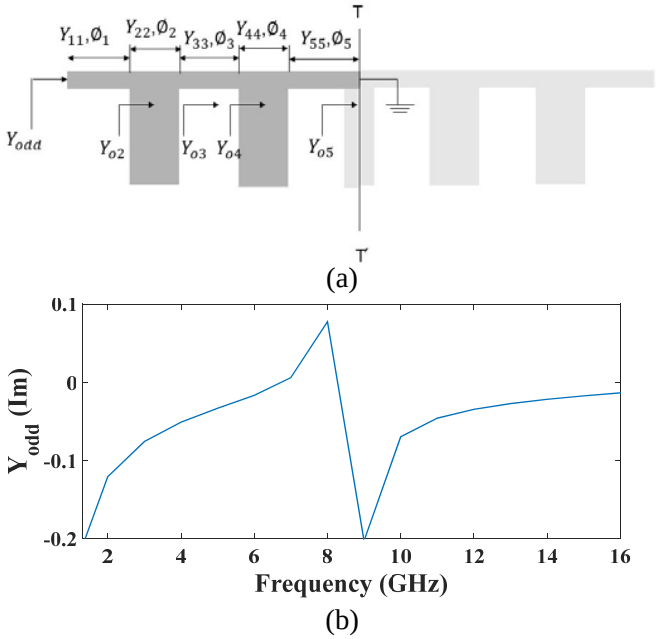

Figure 9. (a) Odd mode equivalent circuit of proposed comb resonator, (b) graphical perspective of odd mode resonance.

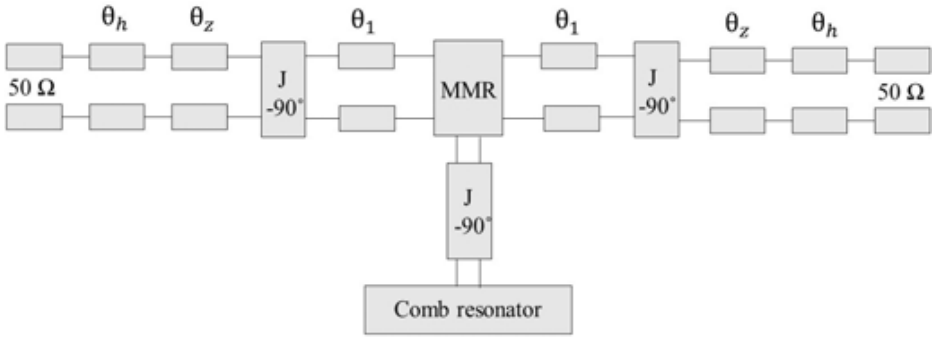

Figure 10. Admittance model of the complete notched band filter.

equations can be presented by Equation (5) where characteristics admittances Y_1, Y_2, ..., Y_5 will be substituted by Y_{11}, Y_{22}, ..., Y_{55}; electrical lengths θ_1 to θ_5 will be substituted by ϕ_1 to ϕ_5; intermediate input admittance Y_{in2}, ..., Y_{in5} will be substituted by Y_{o2}, ..., Y_{o5}, and $Y_{in,even}$ by Y_{odd} respectively while taking $Y_{o5} = -jY_{55}\cot\phi_5$. The graphical portrayal of the resonance for notch frequency obtained from the odd mode analysis of the comb resonator is depicted in Fig. 9(b). Moreover, the admittance model of the whole circuit is established in Fig. 10. Here stubs are indicated by their electrical lengths except for the MMR and comb resonator. In order to demonstrate the coupling functioning between the interconnected structures or resonators as well as the virtual ground effect between them, J-inverter circuits are used. Here J is real and characterized as the inverter admittance.

3.3. Simulation Results and Measurement

The significance of aperture in the ground plane of the design to reduce the insertion loss and return loss levels is illustrated in Fig. 11(a) and Fig. 11(b).

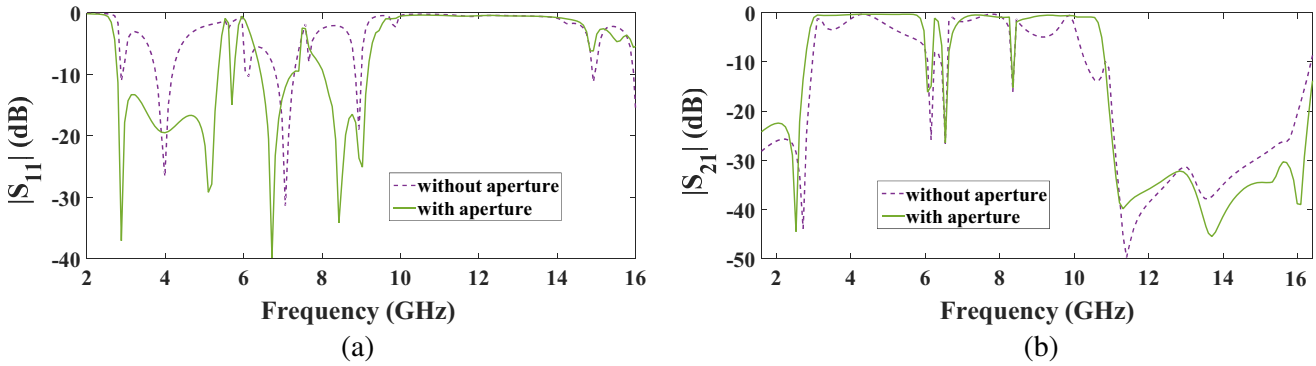

Figure 11. Response of S parameters with and without using apertures, (a) variation in magnitude of $|S_{11}|$, (b) variation in magnitude of $|S_{21}|$.

Next, Fig. 13(a) discusses the ultimate filter responses expressed by $|S_{11}|$ and $|S_{21}|$ magnitude plots reported by the design proposed in Fig. 8. Three notches are developed at 6 GHz, 6.53 GHz, and 8.35 GHz along with a wide 3 dB passband of 7.86 GHz extending from 2.86 GHz to 10.72 GHz. Characteristics of notches are listed in Table 1. The insertion loss in the passband is measured as 0.3 dB to 0.5 dB before the first notch frequency at 6 GHz, 0.44 dB to 0.97 dB between the second and third notches, and 0.5 dB to 0.85 dB after the third notch at 8.35 GHz. A low return loss of −13.27 dB also makes the $|S_{11}|$ characteristics more attractive. Establishing high-frequency selectivity is accomplished also by the existence of two transmission zeros having a high rejection level at either side of the passband. Lower transmission zero is reported at 2.48 GHz having an attenuation level of −44.39 dB, and the upper transmission zero possessing a rejection level of −39.73 dB has appeared at 11.31 GHz. Further, it can be easily perceived from the $|S_{21}|$ traces that the stopband specifications procured by the design are satisfactory and well maintained according to FCC regulations. The lower stopband region has been spread from 0 to 2.48 GHz with an attenuation of more than 22 dB, and the upper stopband is 5.37 GHz

Table 1. Properties of developed notches.

Notch frequency (GHz)	Notch attenuation (dB)	−10 dB passband (GHz)	FBW at −10 dB (%)
6.06	−16.16	6.01–6.19	1.47
6.53	−26.47	6.46–6.62	1.22
8.35	−15.22	8.31–8.39	0.47

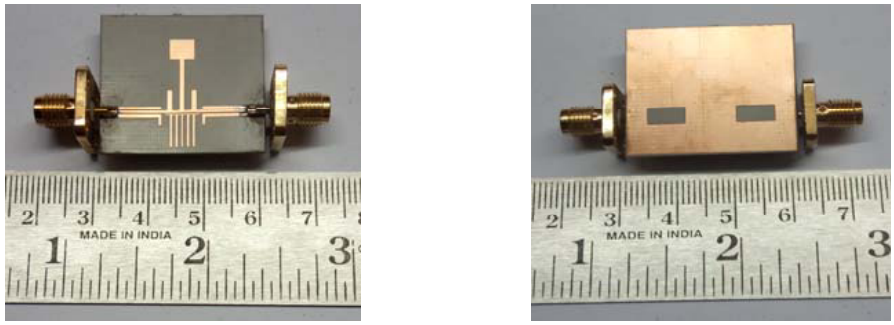

(a) (b)

Figure 12. Fabricated notched band UWB filter, (a) top view, (b) bottom view.

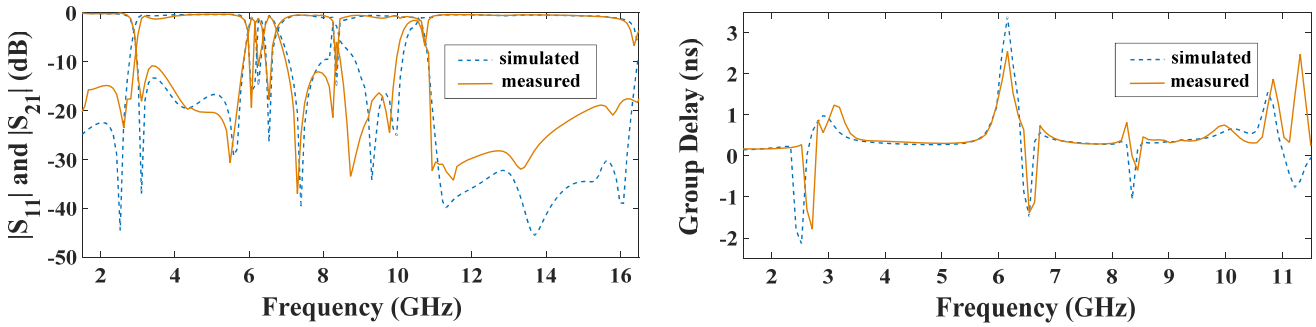

(a) (b)

Figure 13. Comparison of the simulated and measured responses of the filter, (a) S parameters, (b) group delay.

wide at −20 dB attenuation level ranging from 10.97 GHz to 16.34 GHz, with a maximum rejection level greater than 30 dB. The filter measures a high selectivity factor of 0.92. Selectivity factor is computed from the filter passband ratio calculated at −3 dB to passband expanded at −30 dB. A nearly flat group delay referred to Fig. 13(b) is obtained throughout the passband except at the notches, and its variation is calculated as 0.28 ns to 0.45 ns.

After successful simulation in software, the proposed filter is fabricated using Arlon substrate. Both the top view and bottom plane view of the fabricated prototype are shown in Fig. 12, where the overall effective area occupied by the fabricated prototype is 22.62 mm × 19.83 mm. For this design, all the filter parameters are calculated based on center frequency $f_c = 6.85$ GHz. Alternatively, the prototype size can be expressed by substrate wavelength λ_g as $0.81\lambda_g \times 0.71\lambda_g$. Here the value of λ_g is deduced from the formula $\lambda_g = (c/f_c)/\sqrt{\varepsilon_r}$ where ε_r indicates substrate permittivity. The ultimate measured filter performances are compared to simulated results in Fig. 13. Measured data almost matches the simulated output.

The operational mechanism for both the bandpass filter layout presented in Fig. 2 and Fig. 8 is described further in Fig. 14 by the surface current distribution through the filters. In this regard three operating frequencies are chosen in such a way that one operating frequency should be smaller than the lower cutoff of the ultra-wideband (3.1 GHz); another should be greater than the upper cut off frequency (10.6 GHz); and the last one should be at the center frequency of the band (6.85 GHz) namely 2 GHz, 6.85 GHz, and 14 GHz. At 2 GHz and 14 GHz surface current is unable to pass through the structure and is mainly spotted to be concentrated near the input port and the MMR, but at 6.85 GHz it is heavily concentrated on the uniform impedance resonator and stepped impedance resonator as referred in Fig. 14(b) and also noticed to be distributed through the structure from the input port to the output port.

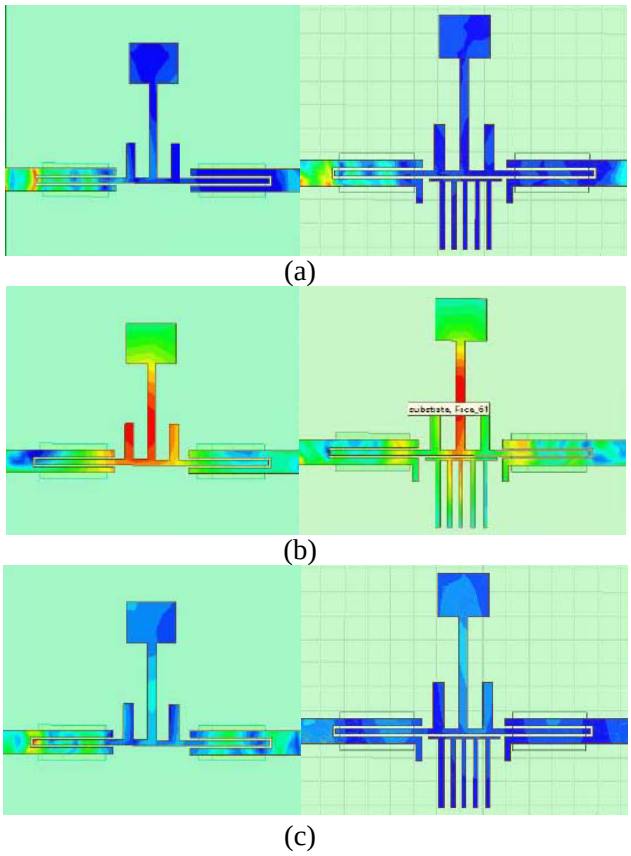

Figure 14. Surface current distribution of the filter at (a) 2 GHz, (b) 6.85 GHz, (c) 14 GHz.

Table 2. Comparison of performance with the available filters.

Ref.	ε_r/t (mm)	IL (dB)	USB (GHz)/ Attenuation (dB)	No of notches	Notch frequency (GHz)/ attenuation (dB)	Size ($\lambda_g \times \lambda_g$)
[18]	2.2/0.787	< 1	4.5/15	1	5/$>$ 40	0.67×0.46
[19]	4.4/0.8	< 0.87–< 1.8	7/15.8	2	6.1/$>$ 15.5, 8.1/$>$ 15.5	1.01×0.76
[20]	4.4/0.8	N.A	5/20	2	4.55/$>$ 15.5, 8.07/$>$ 15.5	1.01×0.76
[21]	4.4/1.6	< 3	0.5/10	1	5.5/32	1.82×1.53
[22]	3.48/0.5	1.3	20/20	3	2.87/33, 5.69/16, 6.5/13	1.44×0.49
[26]	3.66/0.762	0.4	N.A	3	3.3/28, 5.1/19, 8.3/15	1.48×0.52
[27]	10.8/0.635	1.1–1.4	$>$ 5/20	3	5.6, 6.42, 8.03, $>$ 19	1.09×0.69
[28]	2.2/0.787	0.7–2.4	9/10	1	5.2/22.7	1.09×0.44
[29]	3.38/1	0.8	N.A	2	3.5/25.2, 7.5/17.3	1.34×0.41
This paper	2.5/0.8	0.3–0.97	5.37/20	3	6/16.16, 6.53/26.47, 8.35/15.22	0.81×0.71

The proposed notched band bandpass filter output characteristics are compared in Table 2 with the available recent filters found in the literature. Here column wise entries stand for substrate dielectric constant and thickness in mm, insertion loss in dB, upper stopband in GHz with attenuation in dB, number of notches, notch frequency in GHz and notch attenuation in dB, and finally the filter size, measured in substrate guided wavelength which are calculated at center frequency 6.85 GHz respectively.

From the comparison table, it is clearly visible that achieved band characteristics by the proposed filter are highly competitive.

4. CONCLUSION

The proposed triple notch UWB bandpass filter having a 7.86 GHz broad passband ranging from 2.86 GHz to 10.72 GHz achieves a high fractional bandwidth (FBW) of 115.76%. Implementing interdigital couple line extension and a comb shape resonator to the modified MMR structure, in addition to the generation of three notches at 6 GHz, 6.53 GHz, and 8.35 GHz with attenuation levels −16.16 dB, −26.47 dB, and −15.22 dB, respectively, filter performances are also improved for different filter properties. For instance, filter return loss is reduced by 1.05 dB compared to initially proposed plain UWB bandpass filter in this paper. Further, the 5.37 GHz wide upper stopband ranging from 10.97 GHz to 16.34 GHz acquires a bandwidth which is 430 MHz wider than that obtained by the UWB filter proposed without adding notch producing structure, though both the designs satisfactorily maintained FCC specification that the magnitude of $|S_{21}|$ would be less than or equal to −10 dB at 10.6 GHz to 14 GHz for indoor applications. Besides, the filter is highly selective possessing a high skirt factor of 0.92 which implies that the filter is able to repress the signal out of the passband sharply. The filter geometry brings two transmission zeros at two edges of the passband which in turn prompts a swift transition between passband and stopband satisfying the salient characteristics of the UWB bandpass filter. So concisely along with compact size, simple structure, and proper impedance matching, the proposed UWB bandpass filter exhibits good in-band and out-of-band characteristics which justifies the appropriateness of this filter to be used in the UWB communication system.

REFERENCES

1. "Revision of Part 15 of the Commission's rules regarding ultra-wideband transmission system," FCC, Washington, DC, Tech. Rep. ET-Docket 98-153, Apr. 2002.
2. Zhu, L., S. Sun, and W. Menzel, "Ultra-wideband (UWB) bandpass filters using multiple-mode resonator," *IEEE Microw. Wireless Compon. Lett.*, Vol. 15, No. 11, 796–798, Nov. 2005.
3. Jiang, Y., W. Tang, Y. Shi, P. Zhou, and L. Feng, "Compact and low insertion loss UWB on-chip bandpass filter using coupled meanderedline," *Microw. Opt. Technol. Lett.*, 1–7, 2020.
4. Zeng, J., X. Li, and Z. Qi, "UWB bandpass filter with compact size and wide upper stopband," *Microw. Opt. Technol. Lett.*, 1–5, 2019.
5. Kuo, T. N., S. C. Lin, and C. H. Chen, "Compact ultra-wideband bandpass filter using composite microstrip-coplanar-waveguide structure," *IEEE Trans. Microwave Theory Tech.*, Vol. 54, 3772–3778, Oct. 2006.
6. Shaman, H. and J.-S. Hong, "Asymmetric parallel-coupled lines for notch implementation in UWB filters," *IEEE Microw. Wireless Compon. Lett.*, Vol. 17, No. 7, 516–518, Jul. 2007.
7. Chu, Q. X. and X. K. Tian, "Design of UWB bandpass filter using stepped-impedance stub-loaded resonator," *IEEE Microw. Wireless Compon. Lett.*, Vol. 20, No. 9, 501–503, Sep. 2010.
8. Chakraborty, P., P. P. Shome, A. Deb, A. Neogi, and J. R. Panda, "Compact configuration of open ended stub loaded multi-mode resonator based UWB bandpass filter with high selectivity," *IEEE 8th International Conference on Signal Processing and Integrated Networks (SPIN)*, 2021.
9. Shome, P. P., T. Khan, S. K. Koul, and Y. M. M. Antar, "Two decades of UWB filter technology: From elementary designs-to-recent developments," *IEEE Microwave Magazine*, Vol. 22, No. 8, 1–20, Aug. 2021.
10. Shome, P. P. and T. Khan, "A compact design of circular-ring shaped MMR based bandpass filter for UWB applications," *Proc. of the 2019 IEEE Asia-Pacific Microwave Conference (APMC)*, Singapore, Dec. 2019.
11. Gomez-Garcia and J. I. Alonso, "Systematic method for the exact synthesis of ultra-wideband filtering responses using high-pass and low-pass sections," *IEEE Trans. Microwave Theory Tech.*, Vol. 54, No. 10, 3751–3764, Oct. 2006.

12. Song, Y., G. M. Yang, and W. Geyi, "Compact UWB bandpass filter with dual notched bands using defected ground structures," *IEEE Microw. Wireless Compon. Lett.*, Vol. 24, No. 4, 230–232, Apr. 2014.
13. Sarkar, D., T. Moyra, and L. Murmu, "An ultra-wideband (UWB) bandpass filter with complementary split ring resonator for coupling improvement," *International Journal of Electronics and Communication (AEU)*, Vol. 71, 89–95, 2017.
14. Abbosh, A. M., "Planar bandpass filters for ultra-wideband applications," *IEEE Trans. Microwave Theory Tech.*, Vol. 55, 2262–2269, Oct. 2007.
15. Ghatak, R., P. Sarkar, R. K. Mishra, and D. R. Poddar, "A compact UWB bandpass filter with embedded SIR as band notch structure," *IEEE Microw. Wireless Compon. Lett.*, Vol. 21, No. 5, 261–263, May 2011.
16. Janapala, D. K. and M. Nesasudha, "A compact ultra wide band bandpass filter with dual band notch designed based on composite right/left-handed transmission line unit cell," *Int. J. RF Microw. Comput. Aided Eng.*, 2018.
17. Hsiao, P. Y. and R. M. Weng, "A compact ultra-wideband bandpass filter with WLAN notch band," *Microw. Opt. Technol. Lett.*, Vol. 51, No. 2, 503–507, Feb. 2009.
18. Kumari, P., P. Sarkar, and R. Ghatak, "A multi-stub loaded compact UWB BPF with a broad notch band and extended stopband characteristics," *Int. J. RF Microw. Comput. Aided Eng.*, 2020.
19. Ghazali, A. N., M. Sazid, and S. Pal, "A miniaturized low-cost microstrip-to-coplanar waveguide transition-based ultra-wideband bandpass filter with multiple transmission zeros," *Microw. Opt. Technol. Lett.*, 1–6, 2020.
20. Ghazali, A. N., M. Sazid, and S. Pal, "Multiple passband transmission zeros embedded compact UWB filter based on microstrip/CPW transition," *International Journal of Electronics and Communication (AEU)*, Vol. 129, 1–6, 2021.
21. Sangam, R. S. and R. S. Kshetrimayum, "Notched UWB filter using exponential tapered impedance line stub loaded microstrip resonator," *J. Eng.*, Vol. 2018, No. 9, 768–772, 2018.
22. Wang, C., X. Xi, Y. Zhao, and X. Shi, "Compact tri-notched wideband bandpass filter based on multiple resonances with wide upper stopband," *Microw. Opt. Technol. Lett.*, 1–6, 2020.
23. Makimoto, M. and S. Yamashita, *Microwave Resonators and Filters for Wireless Communication Theory, Design and Application*, Vol. 4, Springer Series in Advanced Microelectronics, 2001.
24. Zhu, L., S. Sun, and R. Li, *Microwave Bandpass Filters for Wideband Communications*, John Wiley & Sons, Inc., 2012.
25. Ansoft Corporation, *Ansoft HFSS* (Version 11), 2007.
26. Basit, A., M. I. Khattak, and M. Alhasan, "Design and analysis of a microstrip planar UWB bandpass filter with triple notch bands for WiMAX, WLAN, and X-band satellite communication systems," *Progress In Electromagnetics Research M*, Vol. 93, 155–164, 2020.
27. Liu, F. and M. Qun, "A new compact UWB bandpass filter with quad notched characteristics," *Progress In Electromagnetics Research Letters*, Vol. 88, 83–88, 2020.
28. Weng, M. H., C. W. Hsu, S. W. Lan, and R. Y. Yang, "An ultra-wideband bandpass filter with a notch band and wide upper bandstop performances," *Electronics*, Vol. 8, 1316, 2019.
29. Sazid, M. and N. S. Raghava, "Planar UWB-bandpass filter with multiple passband transmission zeros," *International Journal of Electronics and Communication (AEU)*, Vol. 134, 1–7, 2021.